International Forum on Aeroelasticity and Structural Dynamics
IFASD 2017
25-28 June 2017 Como, Italy

STATE-SPACE REALIZATIONS AND MODEL REDUCTION OF POTENTIAL-FLOW UNSTEADY AERODYNAMICS WITH ARBITRARY KINEMATICS

Rafael Palacios[1], **Robert J. S. Simpson**[1], **Salvatore Maraniello**[1]

[1] Imperial College, London, SW7 2AZ, United Kingdom
r.palacios@imperial.ac.uk

Keywords: Unsteady Aerodynamics, Aeroelasticity, State-Space Models, Unsteady Vortex-Lattice Method

Abstract: We introduce a nondimensional state-space formulation of the unsteady vortex-lattice method for time-domain aerodynamics. It deals with 2- or 3-dimensional geometries, resolves frequencies up to a spatio-temporal Nyquist limit defined by the wake discretization, and has a convenient form for linearization, model reduction and coupling with structural dynamics models. No assumptions are made relating to the kinematics of the fluid-structure interface (inputs) and use of Joukowski's theorem to compute forces naturally resolves all components of the unsteady aerodynamic forcing (outputs). Linearized expressions are written about arbitrary non-zero reference geometries, velocities and loading distributions and as such yield models that are as general as possible given the assumptions in the underlying fluid mechanics. The implementation is verified against classical solutions in the unsteady aerodynamics, and in aeroelastic stability analysis of cantilever wing configurations.

1 INTRODUCTION

Despite the substantial computational and methodological advances in CFD-based unsteady aerodynamics, analysis methods for loads and aeroelastic analysis heavily relies on potential-flow theory for practical applications. In particular, the doublet-lattice method (DLM) [1,2] has long been the tool of choice for frequency-domain aerodynamics at subsonic speeds for applications in which the structural dynamics can be described in modal space. In the standard formulation only induced-velocities, kinematics and resulting forces that are normal to the free-stream are resolved, and any contribution to the unsteady aerodynamics from the steady-state loading distribution is lost [3]. Also, an infinite flat wake that is parallel to the free-stream flow is assumed, which has prevented the method from being applied in problems where this is not a reasonable assumption, such as wind-turbine aeroelasticity [4]. When time-domain models are required, rational function approximations (RFA) of the DLM unsteady aerodynamics are needed [5–7]. In this approach the aerodynamic lag effect, which arises from convection of vorticity downstream in the wake, is approximated in the frequency domain using a least-squares fit.

An alternative approach for incompressible flows was proposed by Hall [8], who wrote a linearized form of the unsteady vortex-lattice equations in state-space form, thus directly obtaining time-domain models. Eigenanalysis of his equations, and aeroelastic equations that used the same fluid model, revealed the structure of eigenvalues underlying the unsteady aerodynamics model and their interaction with structural dynamics degrees-of-freedom [9, 10]. Murua [11]

has more recently developed a more general approach in which induced-drag, in-plane motions, and the effects of steady-state aerodynamic loading were captured, using a UVLM linearized in the degrees-of-freedom of a beam finite-element model. This model was then shown to successfully predict the characteristics of T-tail flutter [12], which depend strongly on static loading and in-plane vibrations and are not captured by the standard DLM.

One potential drawback of using vortex-based methods to directly formulate linear time-domain models is the large number of degrees-of-freedom required to discretize the wake in a converged model. The usual assumption is that vorticity in the discrete wake moves downstream one element per time step. Therefore, the streamwise discretization of the wake sets the temporal discretization of the dynamics in the problem. A small wake spacing will therefore resolve a large frequency range, but at a large cost. If the UVLM equations are linearized, this can be addressed using standard methods of model order reduction. This was first proposed by Hall [8], who projected the equations onto a reduced set of aerodynamic eigenstates, and proceeded by Baker *et al.* [13] who used balanced realizations. Rule *et al.* [14] subsequently compared balanced realizations with direct projection on the system eigenvalues and showed a much better performance for a given system size. This has been recently extended to unsteady aerodynamic problems around non-zero reference conditions by Hesse *et al.* [15].

Simpson *et al.* [16] have recently shown that Joukowski's theorem becomes necessary to compute all three components of the aerodynamic force for problems with arbitrary kinematics. This will be further explored here by presenting the full linearisation of the resulting UVLM formulation. No assumptions will be made relating to the kinematics of the fluid-structure interface and all components of the unsteady aerodynamic forcing are resolved. Furthermore, the linearized equations will be built in nondimensional form, which will scale the aerodynamic loading with the reference dynamic pressure. This will facilitate efficient aeroelastic analyses across the (incompressible) flight envelope. The rest of the paper is structured as follows: A discrete-time state-space description of unsteady aerodynamics with arbitrary kinematics is first outlined in section 2, which is followed by a linearisation around an arbitrary reference configuration, so as to include the effect of non-zero loading, deformed geometries and arbitrary perturbations on the wing kinematics. A brief description on the aeroelastic models using these aerodynamic models is then presented in section 3. The linearized aerodynamics are then exercised in problems of the two-dimensional unsteady aerodynamics of aerofoils and aeroelastic stability of cantilever wings in section 4. Balanced realizations are finally included to demonstrate the potential for model reduction of the proposed approach.

2 THREE-DIMENSIONAL UNSTEADY AERODYNAMICS WITH ARBITRARY KINEMATICS

A discrete-time state-space description of the nonlinear unsteady vortex-lattice-based aerodynamics in nondimensional form is first outlined in this section, followed by the linearization around arbitrary reference conditions. Lifting surfaces will be discretized using a lattice of quadrilateral vortex rings. The description here is done for a single wing, as shown in figure 1, although this can be easily generalized for multiple surfaces [11]. A reference velocity V is considered for nondimensionalization, which will correspond to the forward-flight velocity in the reference condition for linearization (or to the reference blade tip velocity in wind-turbine aerodynamics). The reference length will be a typical semi-chord, b (e.g. at the wing root). This results in the usual scaling of time b/V found in aeroelastic applications. We will refer to t the physical time and $s = tV/b$ the reduced time.

2.1 Lattice discretization

Consider a lifting surface with M rings in the chordwise direction and N rings in the spanwise direction, and $K = MN$. The corresponding wake lattice has $K_w = M_w N$ rings with $M_w >> M$. Each of the vortex rings has a scalar circulation strength, after normalization with bV these are collected in vectors $\boldsymbol{\Gamma} \in \mathbb{R}^K$ and $\boldsymbol{\Gamma_w} \in \mathbb{R}^{K_w}$ that correspond to the surface and wake nondimensional vorticity distributions, respectively.

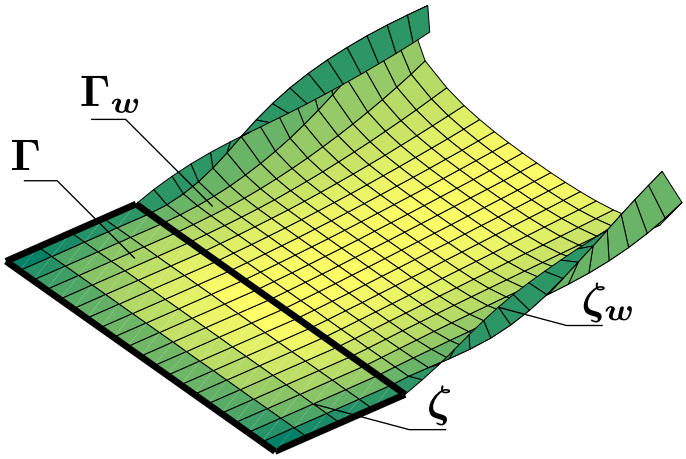

Figure 1: Vortex lattice geometry and circulation distribution.

The instantaneous lattice geometry is described by $K_\zeta = (M+1)(N+1)$ lattice vertices on the surface with $K_{\zeta_w} = (M_w+1)(N+1)$ in the wake. The nondimensional coordinates of those points, given with respect to a certain inertial reference frame, will be $\boldsymbol{\zeta}(t) \in \mathbb{R}^{3K_\zeta}$ and $\boldsymbol{\zeta_w}(t) \in \mathbb{R}^{3K_{\zeta_w}}$ for the surface and wake geometries, respectively. In particular, the time history of the wing kinematics, $\boldsymbol{\zeta}(t)$, is assumed to be known, while the wake is in general assumed to move according to the local flow velocity (i.e., a *free wake*).

Moreover, a background fluid velocity field is also defined at both the surface and the wake. This may include the presence of a mean flow, atmospheric turbulence and other spatially and/or temporally varying features. It will be defined by a vector of the three components of the instantaneous background flow velocity at the lattice vertices, that is, $\boldsymbol{\nu}(t) \in \mathbb{R}^{3K}$ and $\boldsymbol{\nu}_w(t) \in \mathbb{R}^{3K_\zeta}$ for the surface and wake lattice, respectively.

Using this description, the instantaneous induced velocity field generated by the vortex lattice is obtained applying the Biot-Savart law to each side of the vortex rings [17]. This is used in particular to enforce the non-penetrating boundary condition on the lifting surfaces, which is done at collocation points at the centre of each vortex ring. The induced velocity field at each collocation point is projected along the local normal vector to the surface. Consequently, the non-penetration condition can be expressed, at the discrete time step $n+1$, as

$$\boldsymbol{\mathcal{A}}(\boldsymbol{\zeta}^{n+1})\boldsymbol{\Gamma}^{n+1} + \boldsymbol{\mathcal{A}_w}(\boldsymbol{\zeta}^{n+1}, \boldsymbol{\zeta_w}^{n+1})\boldsymbol{\Gamma_w}^{n+1} + \boldsymbol{W}(\boldsymbol{\zeta}^{n+1})\left(\boldsymbol{\nu}^{n+1} - \boldsymbol{\zeta}'^{n+1}\right) = 0. \tag{1}$$

where $\boldsymbol{\mathcal{A}}(\boldsymbol{\zeta}) \in \mathbb{R}^{K\times K}$ and $\boldsymbol{\mathcal{A}_w}(\boldsymbol{\zeta}, \boldsymbol{\zeta_w}) \in \mathbb{R}^{K\times K}$ are the aerodynamic influence coefficient matrices corresponding to wing and wake, and the matrix $\boldsymbol{W}(\boldsymbol{\zeta} \in \mathbb{R}^{K\times 3K_\zeta}$ projects the kinematic and background fluid velocities, given at the vertex corners, along the normal vectors at the collocation points. In particular, a bilinear interpolation is used for the velocities within each vortex ring. Note that the coefficients terms depending of the Biot-Savart law ($\boldsymbol{\mathcal{A}}$ and $\boldsymbol{\mathcal{A}_w}$) will

need in general to be updated at every time step for wings undergoing large geometry changes, which introduced a nonlinearity into the problem. In general, the interpolation matrix $\boldsymbol{W}$ will also need updating to account for the deformation of the vortex rings, although in practice that can be often neglected. Finally, $(\cdot)'$ indicates the derivative with respect to reduced time, s.

2.2 Wake model

Unsteady effects are included through convection of the wake coordinates $\boldsymbol{\zeta_w}$ and circulation $\boldsymbol{\Gamma_w}$ in the fixed reduced time-step Δs. The convection of the wake lattice is given by [11]

$$\boldsymbol{\zeta}_{\boldsymbol{w}}^{n+1} + \boldsymbol{C}_{\boldsymbol{\zeta}}\boldsymbol{\zeta}^{n+1} = \boldsymbol{C}_{\boldsymbol{\zeta_w}}\boldsymbol{\zeta}_{\boldsymbol{w}}^{n} + \Delta s\left(\boldsymbol{\mathcal{A}_1}(\boldsymbol{\zeta}^n, \boldsymbol{\zeta}_{\boldsymbol{w}}^n)\boldsymbol{\Gamma}^n + \boldsymbol{\mathcal{A}_2}(\boldsymbol{\zeta}_{\boldsymbol{w}}^n)\boldsymbol{\Gamma}_{\boldsymbol{w}}^n + \boldsymbol{\nu}_{\boldsymbol{w}}^n\right) , \tag{2}$$

where $\boldsymbol{C}_{\boldsymbol{\zeta}} \in \mathbb{N}^{3K_{\zeta_w}\times 3K_{\zeta}}$ is a sparse, constant matrix that joins the wake lattice with the trailing-edge of the surface lattice at the current time step, while $\boldsymbol{C}_{\boldsymbol{\zeta_w}} \in \mathbb{N}^{3K_{\zeta_w}\times 3K_{\zeta_w}}$ shifts the elements of $\boldsymbol{\zeta}_w$ downstream by one chordwise row. Matrices $\boldsymbol{\mathcal{A}_1}(\boldsymbol{\zeta}, \boldsymbol{\zeta_w}) \in \mathbb{R}^{3K_{\zeta_w}\times K}$ and $\boldsymbol{\mathcal{A}_2}(\boldsymbol{\zeta_w}) \in \mathbb{R}^{3K_{\zeta_w}\times K_w}$ account for the fluid velocities induced by the surface and wake vortex rings at the wake lattice vertices, respectively, and are obtained again from Biot-Savart law. Including these velocities allows the UVLM to capture wake roll-up.

The convection of circulation strengths can be simply written as

$$\boldsymbol{\Gamma}_{\boldsymbol{w}}^{n+1} = \boldsymbol{\mathcal{C}}_{\boldsymbol{\Gamma}}\boldsymbol{\Gamma}^n + \boldsymbol{\mathcal{C}}_{\boldsymbol{\Gamma_w}}\boldsymbol{\Gamma}_{\boldsymbol{w}}^n, \tag{3}$$

in which $\boldsymbol{\mathcal{C}}_{\boldsymbol{\Gamma_w}} \in \mathbb{N}^{K_w\times K_w}$ is a sparse constant matrix that shifts the wake circulation downstream by one chordwise element. Similarly, $\boldsymbol{C}_{\boldsymbol{\Gamma}} \in \mathbb{N}^{K_w\times K}$ propagates the circulation strength from the trailing-edge at the previous time step into the first row of wake vortex rings. The particular form of Eqs. (2)-(3) corresponds to a first-order, explicit, time-stepping scheme, which is widely used in UVLM implementations [17–19].

2.3 Aerodynamic forces

The aerodynamic forces that arise from the surface's motion through the fluid are developed using the Joukowski method [16]. The forces are divided steady and unsteady contributions. The quasi-steady forcing, including induced-drag and leading-edge suction effects, is obtained from applying Joukowski theorem to each of the segments of the lattice. The unsteady contributions are the added mass terms, which are calculated by applying Bernoulli's equation across the surface.

For each of the $s = 1, \ldots, 4K$ segments the (dimensional) quasi-steady force contribution acting at the midpoint of each segment, $\boldsymbol{f}_s \in \mathbb{R}^3$, can be written as

$$\boldsymbol{f}_s = -\rho V^2 b \widetilde{\boldsymbol{l}_s}\boldsymbol{v}_s\Gamma_k \quad \text{with} \quad k = \left\lfloor \frac{s-1}{4} \right\rfloor + 1, \tag{4}$$

where $\boldsymbol{l}_s$ is the dimensional line segment describing the vortex geometry, and $\boldsymbol{v}_s$ is the fluid-segment relative nondimensional velocity, defined as

$$\boldsymbol{v}_s = \boldsymbol{u}_s^{\boldsymbol{m}} + \boldsymbol{H}_s^{\top}\left(\boldsymbol{\nu} - \boldsymbol{\zeta}'\right), \tag{5}$$

where $\boldsymbol{u}_s^{\boldsymbol{m}}$ is the induced velocity by the vortex lattice at the midpoint of segment and $\boldsymbol{H}_s^{\top}$ linearly interpolates the velocities defined in (1) from the segment vertices to the same midpoint.

When calculating $\boldsymbol{u}_s^m$, it is often the case that the target segment lies on a line collinear with the source vortex segment, and if would seem that the Biot-Savart law would yield infinite induced velocities. However, writing the kernel in terms of small perturbations from the collinear line reveals that induced velocities are identically zero there and have an analytically obtainable gradient. The velocities induced by a segment on itself are singular, however, and are avoided by cutting-off the Biot-Savart kernel, i.e. by setting the velocity to zero.

The added mass terms are directly evaluated at the k-th collocation point as

$$\boldsymbol{f}_{\boldsymbol{u}_k} = \rho V A_k \boldsymbol{n}_k \Gamma'_k, \tag{6}$$

where the product of vortex ring area A_k and normal vector $\boldsymbol{n}_k$ is a quadratic function of the surface geometry. Γ'_k is calculated using backward differencing, in-keeping with the first order approximation.

Gathering the contributions of (4) and (6), the vector of aerodynamic force components, $\boldsymbol{f_a} \in \mathbb{R}^{3K_\zeta}$, defined at the lattice vertices, has the form

$$\boldsymbol{f}_{\boldsymbol{a}}^n = \boldsymbol{H}\boldsymbol{f}^n + \boldsymbol{\Xi}^\top \boldsymbol{f}_{\mathbf{u}}^n \tag{7}$$

in which quasi-steady force contributions, $\boldsymbol{f} \in \mathbb{R}^{12K}$, act at the midpoint of each vortex segment and the unsteady contributions, $\boldsymbol{f}_{\mathbf{u}} \in \mathbb{R}^{3K}$, act at the collocation points. The sparse matrix $\boldsymbol{H} \in \mathbb{R}^{3K_\zeta \times 12K}$ is used to distribute force contributions from the vortex segments to the lattice vertices, and is based on the same bilinear relationships as $\boldsymbol{\Xi}$.

2.4 Discrete-time state-space description

To achieve as general a description of the method as possible, and to avoid assumptions in the subsequent derivation of the linearized surface boundary conditions and aerodynamic forcing, the states and inputs with which the nonlinear form of the UVLM is now described are chosen, respectively, as

$$\hat{\mathbf{x}}_a := [\ \boldsymbol{\Gamma};\ \boldsymbol{\Gamma}';\ , \boldsymbol{\Gamma}_{\boldsymbol{w}};\ \boldsymbol{\zeta}_{\boldsymbol{w}}\ ], \tag{8}$$

and

$$\hat{\mathbf{u}}_a := [\ \boldsymbol{\zeta};\ \boldsymbol{\zeta}';\ \boldsymbol{\nu};\ \boldsymbol{\nu}_{\boldsymbol{w}}\ ]. \tag{9}$$

All of the states and inputs are nondimensional, which allows the unsteady aerodynamics model to be written independently of the free-stream dynamic pressure, and are given in terms of the 3-component vectors that comprehensively describe the geometry and kinematics of the problem (as opposed to the typical scalar values of local panel chord, angle-of-attack, lift force, etc.). This uses therefore the actual instantaneous geometry of the surface and wake, which may be undergoing large dynamic deflections or additionally, in the case of the wake, be subject to roll-up.

Finally, the nonlinear equations introduced above can be written in the form of a discrete-time state-space equation of the form

$$\mathbf{p}(\hat{\mathbf{x}}_a^{n+1}, \hat{\mathbf{u}}_a^{n+1}) = \mathbf{q}(\hat{\mathbf{x}}_a^n, \hat{\mathbf{u}}_a^n), \tag{10}$$

$$\boldsymbol{y}^n = \mathbf{r}(\hat{\mathbf{x}}_a^n, \hat{\mathbf{u}}_a^n). \tag{11}$$

where we have explicitly introduced the dynamic pressure (times two) in the output terms as,

$$\boldsymbol{y} = \frac{1}{\rho V^2} \boldsymbol{f_a} \tag{12}$$

force terms

2.5 Consistent linearization

A linearization of the aerodynamics described by (10) and (11) is now sought which will allow the formulation of linear aeroelastic models with several advantages over the traditional DLM-based approach. Aside from those inherent in any linearization the only assumption made in the development of the linear model is that the wake geometry is frozen, but can take any shape, for example a nonplanar prescribed wake or that obtained from nonlinear time-marching of the aerodynamic equations (1) - (3). The approach is therefore very general: discrete-time state-space models are obtained directly; they include the effects of a nonzero reference condition in all the states and inputs of the model, and; can predict linear induced drag effects. Additionally, the description is independent of any structural model, and yields a formulation that is independent of the free-stream dynamic pressure.

To perform the linearization the circulation states are decomposed as

$$\boldsymbol{\Gamma} = \boldsymbol{\Gamma}_0 + \partial\boldsymbol{\Gamma}, \quad \boldsymbol{\Gamma}_{\boldsymbol{w}} = \boldsymbol{\Gamma}_{\boldsymbol{w}_0} + \partial\boldsymbol{\Gamma}_{\boldsymbol{w}}, \quad \text{and} \quad \boldsymbol{\Gamma}' = \boldsymbol{\Gamma}'_0 + \partial\boldsymbol{\Gamma}', \tag{13}$$

along with the geometric and kinematic variables, which take the form

$$\boldsymbol{\zeta} = \boldsymbol{\zeta}_0 + \partial\boldsymbol{\zeta}, \quad \boldsymbol{\zeta}' = \boldsymbol{\zeta}'_0 + \partial\boldsymbol{\zeta}', \quad \text{and} \quad \boldsymbol{\zeta}_{\boldsymbol{w}} = \boldsymbol{\zeta}_{\boldsymbol{w}_0}, \tag{14}$$

where the $\partial(\cdot)$ symbol indicates small perturbations around arbitrary reference values $(\cdot)_0$. Additionally, the reference background fluid velocity field is decomposed as $\boldsymbol{\nu} = \boldsymbol{\nu}_0 + \partial\boldsymbol{\nu}$. Consequently, the reference velocity V_{ref} must be chosen as a fluid-lattice relative velocity representative of the reference conditions $\boldsymbol{\zeta}'_0$ and $\boldsymbol{\nu}_0$ due to the coupling of spatial and temporal scales in the treatment of the wake.

Linearizing (1), using the definitions of (13) and (14), leads to a general expression for the perturbations in the *normalwash*, which can be written as

$$\begin{aligned} &\frac{\partial(\boldsymbol{\mathcal{A}}\boldsymbol{\Gamma}_0)}{\partial\boldsymbol{\zeta}}\partial\boldsymbol{\zeta}^{n+1} + \boldsymbol{\mathcal{A}}_0\partial\boldsymbol{\Gamma}^{n+1} + \frac{\partial(\boldsymbol{\mathcal{A}}_{\boldsymbol{w}}\boldsymbol{\Gamma}_{\boldsymbol{w}_0})}{\partial\boldsymbol{\zeta}}\partial\boldsymbol{\zeta}^{n+1} + \boldsymbol{\mathcal{A}}_{\boldsymbol{w}_0}\partial\boldsymbol{\Gamma}_{\boldsymbol{w}}^{n+1}\ldots \\ &+\left(\frac{\partial(\boldsymbol{W}\boldsymbol{\nu}_0)}{\partial\boldsymbol{\zeta}} - \frac{\partial(\boldsymbol{W}\boldsymbol{\zeta}'_0)}{\partial\boldsymbol{\zeta}}\right)\partial\boldsymbol{\zeta}^{n+1} + \boldsymbol{W}_0\left(\partial\boldsymbol{\nu}^{n+1} - \partial\boldsymbol{\zeta}'^{n+1}\right) \;=\; 0, \end{aligned} \tag{15}$$

where all the matrices are functions of the nondimensional reference geometry, and terms involving derivatives of AIC matrices are the matrix-valued functions

$$\frac{\partial(\boldsymbol{\mathcal{A}}\boldsymbol{\Gamma}_0)}{\partial\boldsymbol{\zeta}} \in \mathbb{R}^{K\times 3K_\zeta}, \quad \text{and} \quad \frac{\partial(\boldsymbol{\mathcal{A}}_{\boldsymbol{w}}\boldsymbol{\Gamma}_{\boldsymbol{w}_0})}{\partial\boldsymbol{\zeta}} \in \mathbb{R}^{K\times 3K_\zeta}, \tag{16}$$

whose elements are obtained by linearizing the Biot-Savart kernels analytically. In addition, the matrix-valued functions in (15),

$$\frac{\partial(\boldsymbol{W}\boldsymbol{\zeta}'_0)}{\partial\boldsymbol{\zeta}} \in \mathbb{R}^{K\times 3K_\zeta}, \quad \text{and} \quad \frac{\partial(\boldsymbol{W}\boldsymbol{\nu}_0)}{\partial\boldsymbol{\zeta}} \in \mathbb{R}^{K\times 3K_\zeta}, \tag{17}$$

give the perturbations in normalwash due to changes in the lattice geometry, and, in particular, any changes in orientation of the surface normal vectors. Note that the costly evaluation of third-order tensors in (16) - (17) is avoided by analytically differentiating the corresponding matrix-vector products directly.

The second equation required for the linear model describes the propagation of circulation through the wake, and is given by the linearization of (3) as

$$\partial\boldsymbol{\Gamma}_{\boldsymbol{w}}^{n+1} = \boldsymbol{\mathcal{C}}_{\boldsymbol{\Gamma}}\partial\boldsymbol{\Gamma}^{n} + \boldsymbol{\mathcal{C}}_{\boldsymbol{\Gamma}_{\boldsymbol{w}}}\partial\boldsymbol{\Gamma}_{\boldsymbol{w}}^{n}, \tag{18}$$

where the matrices keep their original definitions. Finally, perturbations of the rate-of-change of circulation strengths on the body are calculated using the backwards difference formula

$$\Delta s\partial\boldsymbol{\Gamma}'^{n+1} = \partial\boldsymbol{\Gamma}^{n+1} - \partial\boldsymbol{\Gamma}^{n}. \tag{19}$$

Defining the *linear*[1] aerodynamic state vector as

$$\mathbf{x}_a := [\, \partial\boldsymbol{\Gamma};\ \ \partial\boldsymbol{\Gamma}_{\boldsymbol{w}};\ \ \partial\boldsymbol{\Gamma}' \,], \tag{20}$$

and the linear inputs as

$$\mathbf{u}_a := [\, \partial\boldsymbol{\zeta}';\ \ \partial\boldsymbol{\zeta};\ \ \partial\boldsymbol{\nu} \,], \tag{21}$$

the linearized equations (15), (18) and (19) can be written in the state-space descriptor form

$$\boldsymbol{E}_a\mathbf{x}_a^{n+1} = \boldsymbol{F}_a\mathbf{x}_a^{n} + \boldsymbol{G}_a\mathbf{u}_a^{n+1}, \tag{22}$$

where the matrices $\boldsymbol{E}_a, \boldsymbol{F}_a \in \mathbb{R}^{(2K+K_w)\times(2K+K_w)}$ have the form

$$\boldsymbol{E}_a = \begin{bmatrix} \boldsymbol{\mathcal{A}}_0 & \boldsymbol{\mathcal{A}}_{\boldsymbol{w}_0} & 0 \\ 0 & \boldsymbol{\mathcal{I}}_{K_w} & 0 \\ -\boldsymbol{\mathcal{I}}_K & 0 & \Delta s\boldsymbol{\mathcal{I}}_K \end{bmatrix} \tag{23}$$

and

$$\boldsymbol{F}_a = \begin{bmatrix} 0 & 0 & 0 \\ \boldsymbol{\mathcal{C}}_{\boldsymbol{\Gamma}} & \boldsymbol{\mathcal{C}}_{\boldsymbol{\Gamma}_{\boldsymbol{w}}} & 0 \\ -\boldsymbol{\mathcal{I}}_K & 0 & 0 \end{bmatrix} \tag{24}$$

in which $\boldsymbol{\mathcal{I}}_K$ is a $K \times K$ unit matrix, and the input matrix for the state equation, $\boldsymbol{G}_a \in \mathbb{R}^{(2K+K_w)\times 9K_\zeta}$, has the form

$$\boldsymbol{G}_a = \begin{bmatrix} \boldsymbol{W}_0 & \left(-\frac{\partial(\boldsymbol{\mathcal{A}}\boldsymbol{\Gamma}_0)}{\partial\boldsymbol{\zeta}} - \frac{\partial(\boldsymbol{\mathcal{A}}_{\boldsymbol{w}}\boldsymbol{\Gamma}_{\boldsymbol{w}_0})}{\partial\boldsymbol{\zeta}} + \frac{\partial(\boldsymbol{W}\boldsymbol{\zeta}_0')}{\partial\boldsymbol{\zeta}} - \frac{\partial(\boldsymbol{W}\boldsymbol{\nu}_0)}{\partial\boldsymbol{\zeta}}\right) & -\boldsymbol{W}_0 \\ 0 & 0 & 0 \\ 0 & 0 & 0 \end{bmatrix}. \tag{25}$$

Note that the inputs on the right-hand-side of (22) are, atypically, taken at time $n+1$. This is a consequence of (1), and hence (15), being elliptic equations – i.e. the effect of a fluid disturbance is felt everywhere instantaneously. Hence, all of the unsteadiness in the fluid response arises from the time-history of instantaneous solutions to (15), typically with time-varying boundary conditions, through the propagation equation (18). Also, since $\boldsymbol{E}_a$ is non-singular, the state-space form $\mathbf{x}_a^{n+1} = \boldsymbol{A}_a\mathbf{x}_a^{n} + \boldsymbol{B}_a\mathbf{u}_a^{n+1}$ can be obtained, if necessary, where $\boldsymbol{A}_a = \boldsymbol{E}_a^{-1}\boldsymbol{F}_a$ and $\boldsymbol{B}_a = \boldsymbol{E}_a^{-1}\boldsymbol{G}_a$. The descriptor form is retained for numerical efficiency however (since $\boldsymbol{E}_a^{-1}$ need rarely be evaluated explicitly).

[1]The linear states and inputs are made distinct from those defined in the nonlinear description, (8) & (9), since the wake geometry is no longer a state of the system and the quantities in (20) & (21) are all perturbations. The $\partial(\cdot)$ symbol is omitted on the left-hand-side of these definitions for notational brevity.

The outputs, $\mathbf{y}_a \in \mathbb{R}^{3K_\zeta}$, are defined to be the perturbations in aerodynamic forces at the lattice vertices and are obtained through linearization of (7), giving

$$\mathbf{y}_a^n = \partial \boldsymbol{f}_a^n = \boldsymbol{H} \partial \boldsymbol{f}^n + \boldsymbol{\Xi}^\top \partial \boldsymbol{f}_{\boldsymbol{u}}^n, \tag{26}$$

where the force perturbations on the s-th segment are

$$\frac{\partial \boldsymbol{f}_s}{\rho V^2 b} \;=\; \widetilde{\boldsymbol{v}_{0_s}} \boldsymbol{l}_{0_s} \partial \Gamma_k \;+\; \Gamma_{0_k} \widetilde{\boldsymbol{v}_{0_s}} \frac{\partial \boldsymbol{l}_s}{\partial \boldsymbol{\zeta}_q} \partial \boldsymbol{\zeta}_q \;-\; \Gamma_{0_k} \widetilde{\boldsymbol{l}_{0_s}} \partial \boldsymbol{v}_s, \tag{27}$$

where $q = 1, \ldots, K_\zeta$ is an index through the lattice vertices, and the variations in velocities at the segment midpoints are expressed as

$$\begin{aligned} \partial \boldsymbol{v} \;=\; & \boldsymbol{\mathcal{A}}_0^{\boldsymbol{m}} \partial \boldsymbol{\Gamma} \;+\; \frac{\partial (\boldsymbol{\mathcal{A}}^{\boldsymbol{m}} \boldsymbol{\Gamma}_0)}{\partial \boldsymbol{\zeta}} \partial \boldsymbol{\zeta} \;+\; \boldsymbol{\mathcal{A}}_{\boldsymbol{w}_0}^{\boldsymbol{m}} \partial \boldsymbol{\Gamma}_{\boldsymbol{w}} \;+\; \frac{\partial (\boldsymbol{\mathcal{A}}_{\boldsymbol{w}}^{\boldsymbol{m}} \boldsymbol{\Gamma}_{\boldsymbol{w}_0})}{\partial \boldsymbol{\zeta}} \partial \boldsymbol{\zeta} \;\ldots \\ & +\; \boldsymbol{H}^\top \left(\partial \boldsymbol{\nu} - \partial \boldsymbol{\zeta}' \right), \end{aligned} \tag{28}$$

in which the AIC matrices $\boldsymbol{\mathcal{A}}_0^{\boldsymbol{m}} \in \mathbb{R}^{12K \times K}$ and $\boldsymbol{\mathcal{A}}_{\boldsymbol{w}0}^{\boldsymbol{m}} \in \mathbb{R}^{12K \times K_w}$ map the surface and wake circulation distributions to induced velocities at the segment midpoints. The added mass force contribution at each collocation point, from (6), has the linearized form

$$\frac{\partial \boldsymbol{f}_{\mathrm{u}_k}}{\rho V^2} = A_{0_k} \boldsymbol{n}_{k_0} \partial \Gamma'_k + \Gamma'_{0_k} \frac{\partial (A_k \boldsymbol{n}_k)}{\partial \boldsymbol{\zeta}_q} \partial \boldsymbol{\zeta}_q. \tag{29}$$

Gathering the equations (26) - (29) allows a state-space representation of the output equation, which has the form

$$\mathbf{y}_a = \boldsymbol{C}_a \mathbf{x}_a + \boldsymbol{D}_a \mathbf{u}_a, \tag{30}$$

where $\boldsymbol{C}_a \in \mathbb{R}^{3K_\zeta \times (2K + K_w)}$ and $\boldsymbol{D}_a \in \mathbb{R}^{3K_\zeta \times 9K_\zeta}$ can be written as

$$\boldsymbol{C}_a = \left[\; \boldsymbol{H} \left(\boldsymbol{Y_1} - \boldsymbol{Y_3} \boldsymbol{\mathcal{A}}_0^{\boldsymbol{m}} \right), \quad - \boldsymbol{H} \boldsymbol{Y_3} \boldsymbol{\mathcal{A}}_{\boldsymbol{w}_0}^{\boldsymbol{m}}, \;\; \boldsymbol{\Xi}^\top \boldsymbol{Y_4} \; \right], \tag{31}$$

and

$$\begin{aligned} \boldsymbol{D}_a = \Big[\; & \boldsymbol{H} \boldsymbol{Y_3} \boldsymbol{H}^\top, \; \ldots \\ & \boldsymbol{H} \boldsymbol{Y_2} - \boldsymbol{H} \boldsymbol{Y_3} \left(\frac{\partial (\boldsymbol{\mathcal{A}}^{\boldsymbol{m}} \boldsymbol{\Gamma}_0)}{\partial \boldsymbol{\zeta}} + \frac{\partial (\boldsymbol{\mathcal{A}}_{\boldsymbol{w}}^{\boldsymbol{m}} \boldsymbol{\Gamma}_{\boldsymbol{w}_0})}{\partial \boldsymbol{\zeta}} \right) + \boldsymbol{\Xi}^\top \boldsymbol{Y_5}, \; \ldots \\ & - \boldsymbol{H} \boldsymbol{Y_3} \boldsymbol{H}^\top \; \Big], \end{aligned} \tag{32}$$

in which $\boldsymbol{Y_{(1-5)}}$ are relatively-simple block-diagonal or sparse matrices. Since this description is based on linearizations of the three-dimensional form of the Joukowski theorem, (4), no component of the problem kinematics or force distribution is neglected. This means that the effects of arbitrary (small) kinematics – including in-plane motions – are all captured, and that the unsteady induced drag is resolved naturally as a component of the resulting force distribution. Moreover, the only previous linear UVLM to capture such effects was formulated with respect to a subset of the degrees-of-freedom of an underlying beam structural dynamics model [19], whereas this formulation is independent of the kinematic assumption on the fluid-structure interface.

Together with the state equation, (22), the output equation (30) describes the unsteady aerodynamics linearized around an arbitrary reference state. It provides a physics-based formulation for incompressible potential-flow aerodynamics in the time-domain. Note finally, that frequency-domain representations can also be obtained by direct manipulation of the system matrices and the z-transform.

3 INTEGRATION INTO AEROELASTIC MODELS

The unsteady aerodynamic formulation presented above is such that it can be integrated easily with any structural dynamics model. Only two mapping procedures are required to define the fluid-structure interface (FSI): Firstly, transformation from the physical coordinates of the structural model, $\boldsymbol{\eta}$, and their rates of change, $\boldsymbol{\eta}'$, to the displacements and velocities the surface lattice, $\boldsymbol{\zeta}$ and $\boldsymbol{\zeta}'$, denoted $\boldsymbol{T_{as}}$; and secondly, transformation of the force distribution on the surface lattice, $\boldsymbol{f_a}$, to the boundary of the structure, $\boldsymbol{f}$, denoted $\boldsymbol{T_{sa}}$. It is also helpful to note that, providing the structural force distribution and geometry is expressed at coincident locations, the transformation of the linearized structural displacement/rotation field to the surface lattice displacements is simply $\boldsymbol{T_{sa}^\top}$ [20].

The discrete-time aerodynamics of (22) and (30) can then be projected into the generalized coordinates of the structure as

$$\begin{aligned} \boldsymbol{E}_a \mathbf{x}_a^{n+1} &= \boldsymbol{F}_a \mathbf{x}_a^n + \boldsymbol{G}_a \boldsymbol{T}_{as} \boldsymbol{\Phi}_m \mathbf{x}_m^n \\ \boldsymbol{Q}^n &= \boldsymbol{\Phi}^\top \boldsymbol{T}_{sa} \boldsymbol{C_a} \mathbf{x}_a^n + \boldsymbol{\Phi}^\top \boldsymbol{T}_{sa} \boldsymbol{D}_a \boldsymbol{T}_{as} \boldsymbol{\Phi}_m \mathbf{x}_m^n \end{aligned} \tag{33}$$

where $\mathbf{x}_m = [\ \boldsymbol{q}\ ;\ \boldsymbol{q}'\ ]$ is a concatenation of the structure's generalized coordinates, and

$$\boldsymbol{\Phi}_m = \begin{bmatrix} \boldsymbol{\Phi} & 0 \\ 0 & \boldsymbol{\Phi} \end{bmatrix}.$$

3.1 State-space model of beam dynamics

To exemplify the application to aeroelastic analysis in this work a modal model of cantilever beam dynamics is used. Defining the displacements and parameterized rotations along a (beam) reference line as $\boldsymbol{\eta}(x) = [\ \mathbf{r}(x);\ \boldsymbol{\theta}(x)\ ]$, where x is the beam arc-length, a set of mass-orthonormalized modes are assumed such that $\boldsymbol{\eta}(x) = \boldsymbol{\Phi}(x)\boldsymbol{q}$, where $\boldsymbol{q}$ are the modal amplitudes. Thus, using reduced time introduced above, the beam dynamics can be expressed as

$$\left(V^2/b\right) \boldsymbol{q}'' + \boldsymbol{\Omega}^2 \boldsymbol{q} = \rho V^2\, \boldsymbol{Q}(s), \tag{34}$$

where $\boldsymbol{\Omega} = \mathit{diag}\,\{\omega_1, \omega_2, \ldots, \omega_n\}$ is the diagonal matrix of modal frequencies, and $\boldsymbol{Q}(s) = \boldsymbol{\Phi}^\top \boldsymbol{F}(x, s)$ are the normalized generalized forces. Note that as this is a beam description, in which there are rotational degrees of freedom, the notation $\boldsymbol{F}$ is used to denote the forces *and moments* applied along the beam reference line. Since a state-space realization of the aeroelastic equations is desired, (34) is written in first-order form using the definition of $\mathbf{x}_m$ from section 3 and $\bar{\boldsymbol{\Omega}} := \frac{b}{V}\boldsymbol{\Omega} = \mathit{diag}\,\{k_1, k_2, \ldots, k_n\}$, resulting in the continuous-time, linear, time-invariant equations $\mathbf{x}_m' = \mathbf{A}_c \mathbf{x}_m + \mathbf{B}_c \boldsymbol{Q}$ where

$$\mathbf{A}_c = \begin{bmatrix} 0 & -\bar{\boldsymbol{\Omega}}^2 \\ \boldsymbol{I} & 0 \end{bmatrix}, \text{ and } \mathbf{B}_c = \begin{bmatrix} (\rho b^2)\, \boldsymbol{I} \\ 0 \end{bmatrix}.$$

A discrete-time equivalent of this system is then found – with the same sampling period as (22) – by assuming zero-order-hold on the inputs, which gives the discrete-time modal form of the structural dynamics equations as

$$\begin{aligned} \mathbf{x}_m^{n+1} &= \mathbf{A}_m \mathbf{x}_m^n + \mathbf{B}_m \boldsymbol{Q}^n, \\ \mathbf{y}_m^n &= \mathbf{x}_m^n, \end{aligned} \tag{35}$$

where $\mathbf{A}_m = e^{\Delta s \mathbf{A}_c}$ and $\mathbf{B}_m = \mathbf{A}_c^{-1}\left(e^{\Delta s \mathbf{A}_c} - \boldsymbol{I}\right)\mathbf{B}_c$ [21].

A relationship is finally needed between the displacements/rotations of the beam reference line and the displacements of the surface lattice vertices. To facilitate this the aerodynamic discretization is chosen such that there are $j = 1, \ldots, N+1$ cross-sections – assumed to be rigid – that intersect the beam reference line at arc lengths x_j, where each cross section is defined by the $i = 1, \ldots, M+1$ dimensional coordinates, $\boldsymbol{\xi}_{ij} \in \mathbb{R}^3$. Consequently, for the general case in which the beam is deformed in its reference state, the expression

$$\partial\boldsymbol{\zeta}_q = \frac{1}{c}\left(\partial\mathbf{r}_j - \boldsymbol{C}_j^\top \widetilde{\boldsymbol{\xi}}_{ij}\boldsymbol{T}_j\partial\boldsymbol{\theta}_j\right) \tag{36}$$

gives the perturbations in lattice geometry as a linear function of the beam degrees-of-freedom. The matrices $\boldsymbol{C}_j = \boldsymbol{C}(\boldsymbol{\theta}_0(x_j)) \in \mathbb{R}^{3\times3}$ and $\boldsymbol{T}_j = \boldsymbol{T}(\boldsymbol{\theta}_0(x_j)) \in \mathbb{R}^{3\times3}$ are coordinate transformation and tangential operator matrices [22], respectively, and are defined by the orientation of the cross-sections, and the index q is a one-to-one function of the indices (i, j). Conveniently, using (36) to define a transformation $\partial\boldsymbol{\zeta} = \boldsymbol{\Xi}_{as}\partial\boldsymbol{\eta}$, allows the transformation matrix from aerodynamic forces to the forces and moments on the beam to be expressed as $\boldsymbol{T}_{as} = \boldsymbol{\Xi}_{as}^\top \in \mathbb{R}^{6(N+1)\times3K_\zeta}$.

Using the same quantities the velocity perturbations at the lattice vertices can be expressed as

$$\partial\boldsymbol{\zeta}'_q = \frac{1}{c}\left(\partial\mathbf{r}'_j - \boldsymbol{C}_j^\top \widetilde{\boldsymbol{\xi}}_{ij}\boldsymbol{T}_j\partial\boldsymbol{\theta}'_j\right). \tag{37}$$

Finally, the mapping $\boldsymbol{T_{as}} \in \mathbb{R}^{9K_\zeta\times12(N+1)}$ is defined by collecting (36) and (37).

4 NUMERICAL INVESTIGATIONS

In this section the goal is to leverage the form of the new linear model, equations (22) and (30), to investigate the dynamic response of aerofoils and wings, and verify the modelling approach in a comprehensive way. In addition to this, the effects of non-zero reference conditions on the linearized unsteady aerodynamics will be investigated in the context of vibrations and aeroelastic stability of cantilever wings with large deformations in their reference configurations.

4.1 Frequency response of a thin aerofoil with trailing-edge flap

The frequency-domain aerodynamic response of thin aerofoils at zero incidence is now investigated using the linearized model described above for the case of a single chordwise row of panels with very large spanwise aspect ratio. Its inputs, which are perturbations of the lattice geometry and velocities, are written in terms of the pitch angle, α (with time-derivative α'), about the quarter chord, and the angle of a trailing-edge flap, β (with time-derivative β'), hinged at the three-quarter-chord.

Magnitude and phase plots of the lift and moments (also about the quarter-chord) that result from oscillations in these degrees-of-freedom are presented in Figure 2 over a range of reduced frequencies. As the number of vortex rings, M, discretizing the chord is increased the response obtained from the vortex-based method converges to Theodorsen's analytical solution. The reduced time step is set such that the vortex rings in the wake have the same chordwise extent as those on the surface, i.e. $\Delta s = 2/M$, which has the effect of linking the temporal and surface discretizations.

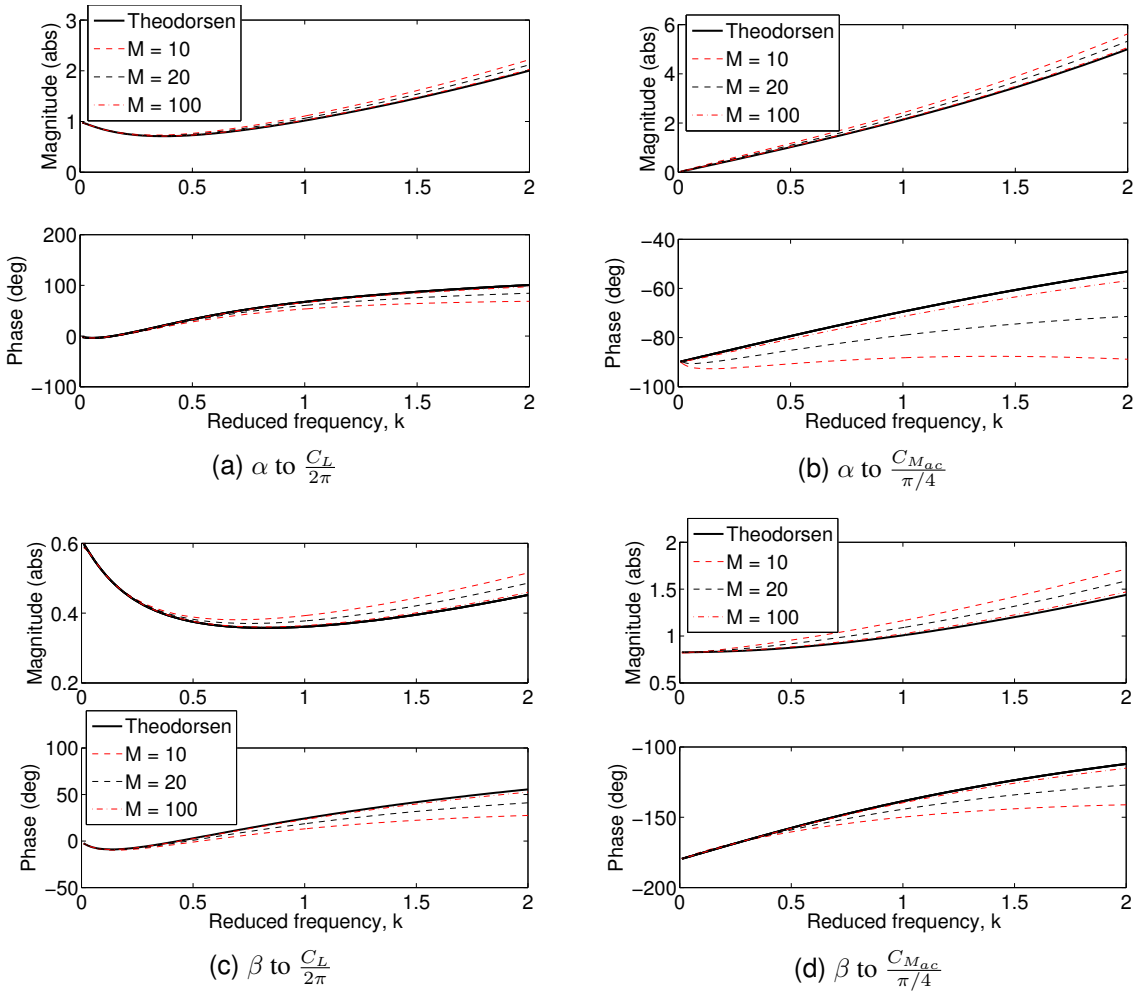

(a) α to $\frac{C_L}{2\pi}$

(b) α to $\frac{C_{M_{ac}}}{\pi/4}$

(c) β to $\frac{C_L}{2\pi}$

(d) β to $\frac{C_{M_{ac}}}{\pi/4}$

Figure 2: Frequency-response between angle of incidence and flap deflection (inputs), and lift and moment coefficients (outputs). Results from analytical models, and the linearized vortex-lattice with $M_w/M = 30$.

The aerofoil is also subject to a travelling vertical gust that moves with the airspeed and has an instantaneous nondimensional upwash $w_g(t)$ at the leading edge. If the upwash due to gusts on the airfoil at time s_n is $\boldsymbol{\nu}_g^n \in \mathbb{R}^{M+1}$, the upwash at time s_{n+1} will be obtained by the lag operator

$$\begin{aligned} \nu_{g,1}^{n+1} &= w_g(s_{n+1}) \\ \nu_{g,j}^{n+1} &= \nu_{g,j-1}^{n} \qquad \text{for} \quad j = 2, \ldots, M+1, \end{aligned} \tag{38}$$

For a given time-history of the gust (38) can be solved alongside the aerodynamic system equations. Augmenting the state-space aerodynamic model with the gust states $\boldsymbol{\nu}_g$, with dynamics given the dynamics of (38), we obtain the response to arbitrary gusts profiles. The frequency-response function of that augmented problem corresponds to Sears' analytical solution to a sinusoidal gust at the leading edge of a thin plate [23]. The lift response obtained by the augmented state-space model is compared to that of Sears in Figure 3.

In both cases, forced and gust response, a relatively slow convergence with the number of chordwise is observed, which is a well-known characteristic of time-domain solutions in unsteady aerodynamics using vortex ring discretizations. The total size of the resulting linear system is dominated by the discretization of the wake, which typically needs to be modelled for over 20 chord lengths to properly incorporate unsteady effects. This calls for methods for model reduction for linear-time-invariant state-space systems, which are readily available. Here, this

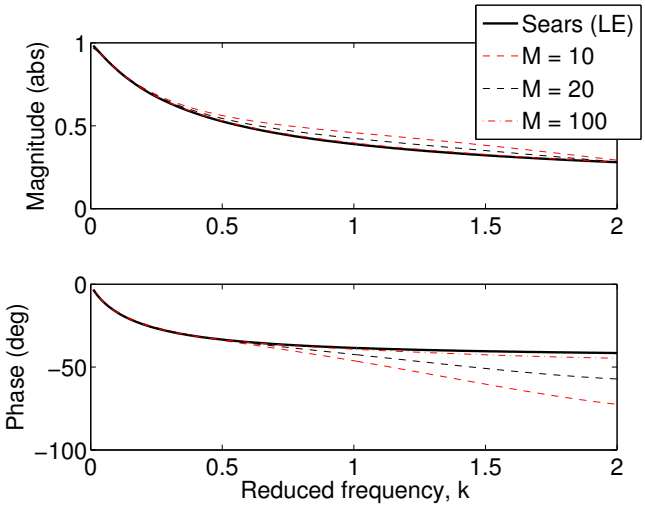

Figure 3: Frequency-response gust velocity and lift coefficient. Results from analytical models, and the linearized vortex-lattice with $M_w/M = 30$.

will be demonstrated using a balanced realization of the system [24].

Figure 4 shows, in logarithmic scale, the first 50 normalized Hankel singular values of the forced-response problem with no gust. As they decrease in amplitude very quickly, only a few balanced states are necessary to represent the system dynamics. This is confirmed in Figure 5, which shows the frequency response functions between inputs and lift and moment coefficients (divided by 2π). The description naturally deal independently with angles and rates and they are present separately. The converged full model solution, with a 30-chord wake and 100 chordwise panels along the aerofoil, has been reduced to systems of dimension N_r =2, 4, and 6. As it can be seen, the full dynamic response of the original converged system (of dimension 3100) at low frequencies can be accurately obtained with a reduced system as small as $N_r = 4$.

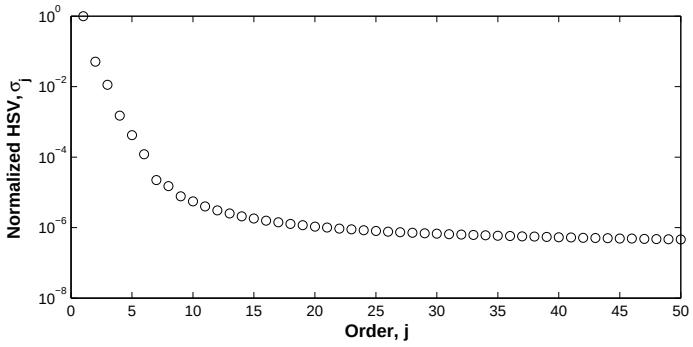

Figure 4: Hankel singular values for a thin aerofoil with pitch/plunge/flap degrees of freedom.

4.2 Dynamic aeroelasticity of cantilever wings

The wing model defined by Goland [25] is finally used to illustrate 3-D results. This is a prismatic cantilever wing with a structural model given by a beam of constant sections described by the parameters in Table 1. The first four natural modes are shown in Figure 6, where the wing surface has been constructed under the assumption of rigid cross-sections. Due to the local pitch-plunge inertial coupling introduced by the offset of the inertial axis from the elastic axis, all of the modes are coupled bending/torsion modes.

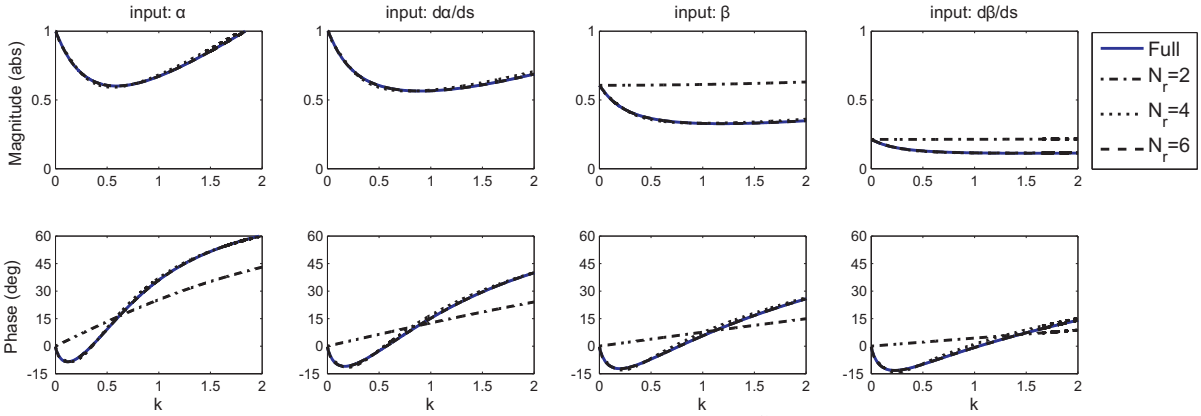

(a) Normalized lift coefficient, $\frac{C_L}{2\pi}$

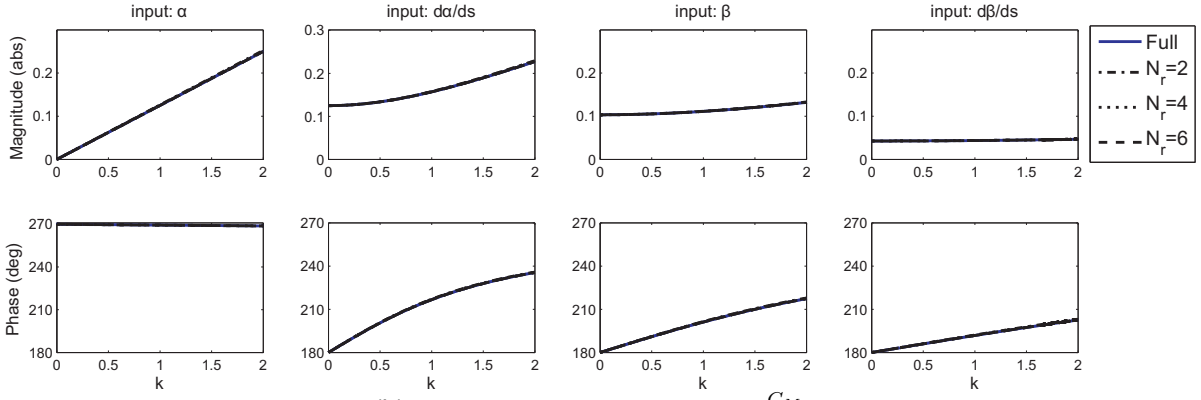

(b) Normalized moment coefficient, $\frac{C_{M_{ac}}}{2\pi}$

Figure 5: Frequency-response functions of the aerofoil problem for balanced residualizations of order N_r.

Convergence of the aerodynamic discretization can now be carried out within the context of the modal beam dynamics. For this purpose the frequency response of (33) is studied in the frequency-domain for different spanwise discretizations in the aerodynamic model, i.e. the number of spanwise vortex rings, N, and shown in Figures 7 & 8. In all combinations of generalized forces and modal amplitudes 40 spanwise vortex rings are required to achieved a converged magnitude and phase response in the modal coordinates.

For verification purposes the flutter characteristics of the Goland wing is now calculated. In the test case the air density is $\rho_\infty = 1.02\ \text{kg}{\cdot}\text{m}^{-3}$, and the wing is at zero incidence. Consequently, as there is zero reference loading at all flight velocities, only one modified aerodynamic model is required to construct aeroelastic models for the entire flight envelope owing to the model's nondimensional form. Thus, in computing successive non-trivial solutions to the eigenproblem

$$\boldsymbol{A}\left(V_\infty\right)\mathbf{x}_i = e^{\Delta t \lambda_i}\mathbf{x}_i \quad \text{for } i = 1, \ \ldots \ , \ n, \tag{39}$$

where $\boldsymbol{A} \in \mathbb{R}^{n\times n}$ is the discrete-time state-transfer matrix of the aeroelastic model with eigenvectors $\mathbf{x}_i = [\ \mathbf{x}_{\mathbf{a}_i};\ \mathbf{x}_{\mathbf{m}_i}\ ]$, only the relatively-small structural dynamics sub-matrices need to be updated. The terms λ_i are continuous-time eigenvalues of the aeroelastic system, which when plotted for a range of free-stream velocities yield root-loci of the coupled system dynamics, as shown in Figure 9.

The converged coupled system has dimension $n = 8808$ with very many highly-damped, predominantly-aerodynamic eigenvalues visible across the whole frequency spectrum, while

chord	1.8288 m
semi-span	6.096 m
elastic axis	33% chord
center of gravity	43% chord
mass per unit length	35.71 kg/m
polar moment of inertia	8.64 kg·m
torsional stiffness	0.99×10^6 N·m^2
bending stiffness	9.77×10^6 N·m^2

Table 1: Goland wing properties. [25]

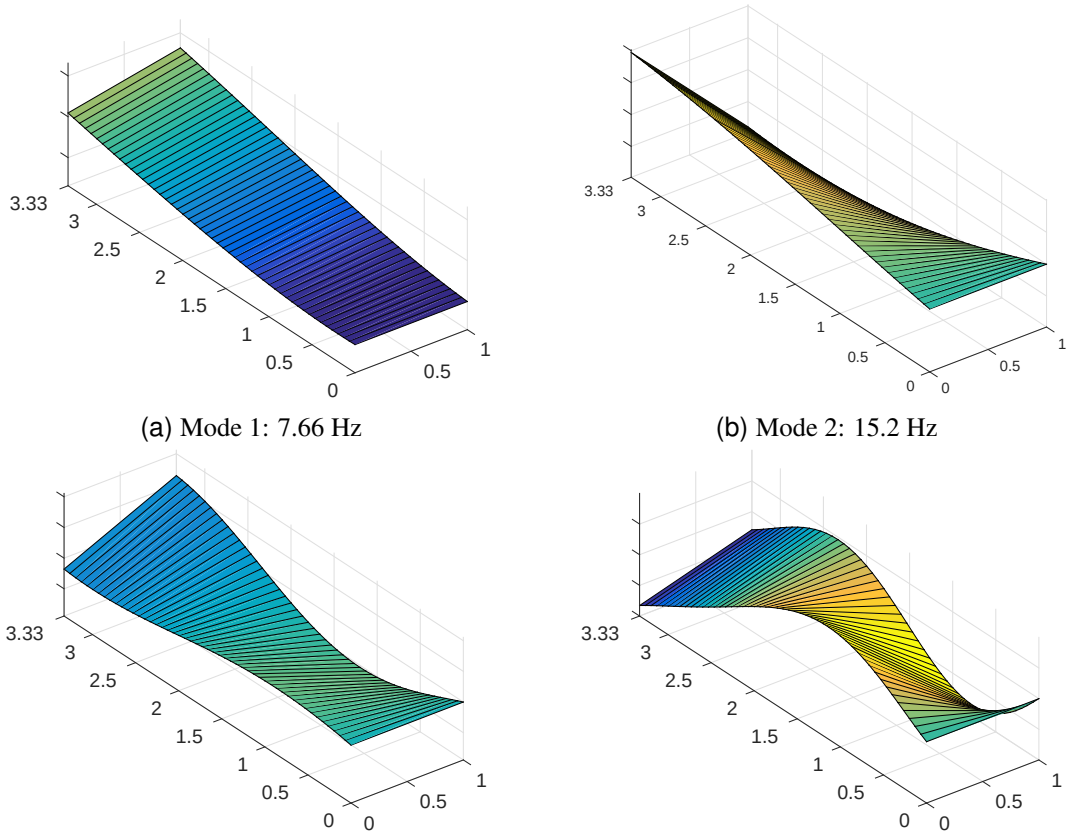

(a) Mode 1: 7.66 Hz

(b) Mode 2: 15.2 Hz

(c) Mode 3: 38.8 Hz

(d) Mode 4: 53.3 Hz

Figure 6: First four natural modes of the Goland wing projected on the aerodynamic lattice.

the critical mode, found in the low-frequency region near the origin in Figure 9(c), originates from the second *in vacuo* structural mode. While capturing all of the eigenvalues shown in Figure 9a is perhaps unnecessary, it is a consequence of the discrete vortex-based method, which, to its advantage, is general and directly gives discrete-time models. A summary of the computed flutter characteristics and a scomparison with the analytical and computational resultsof other authors in Table 2. The results show that at the finest aerodynamic discretization the flutter speed and frequency are converged with less than 1% error, and compare well to results in the literature.

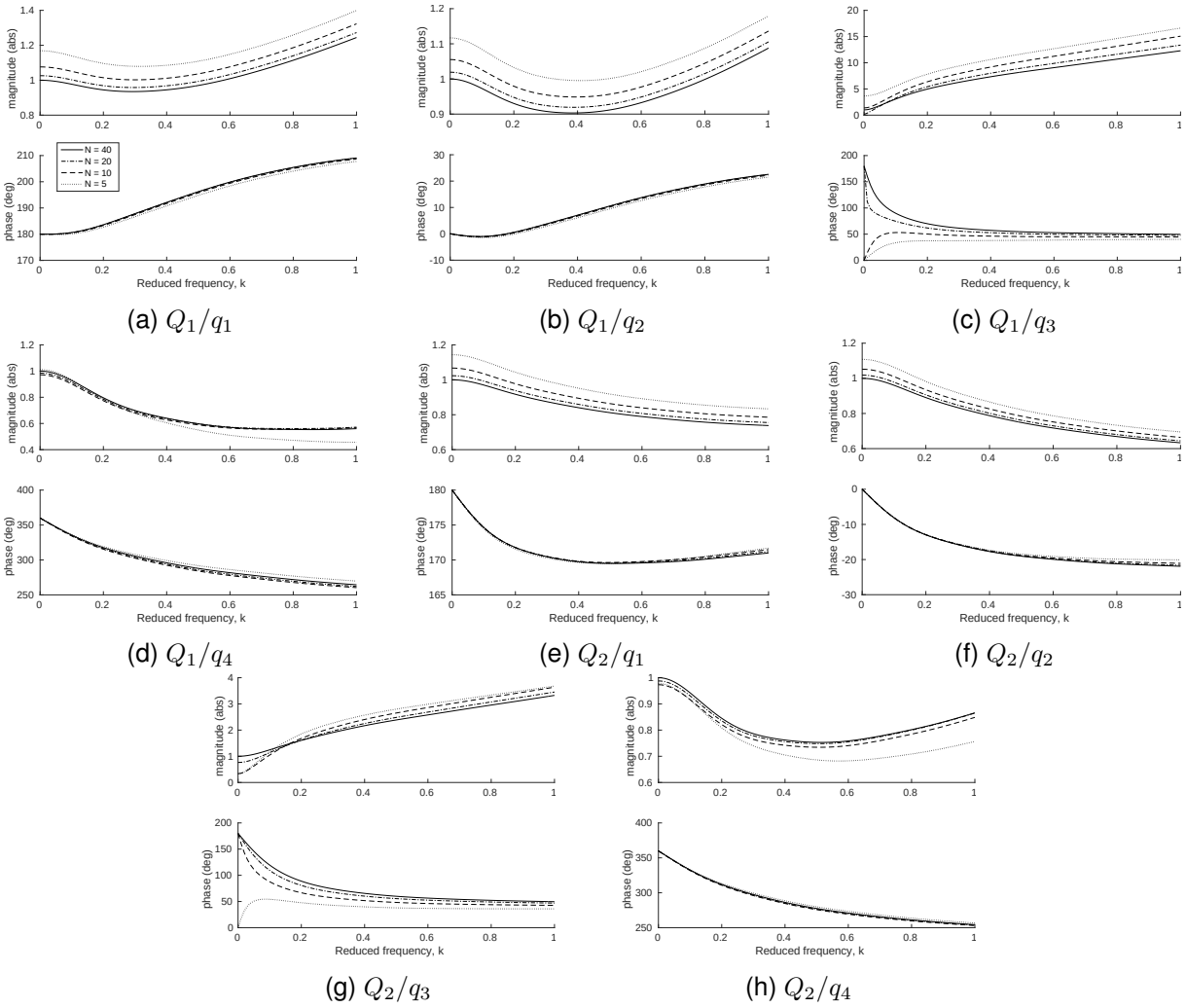

Figure 7: Full-order model frequency responses of the Goland wing aerodynamics for inputs in the first four aeroelastic modes and outputs in the first two modes. Amplitudes normalized by the $N = 40$ steady-state values. Chordwise discretization is $M = 20, M_w = 200$.

Source	Discretization ($M \times N$)	States	V_f, m·s^{-1}	ω_f, Hz
Present	10×20	2200	166.2	10.4
Present	15×30	4950	169.3	10.5
Present	20×40	8800	170.0	10.6
Wang *et al.* [18]	-	-	174.3	-
Hesse and Palacios [26]	16×26	4550	169	11.1

Table 2: Flutter characteristics of the Goland wing calculated with different aerodynamic discretizations.

5 CONCLUSIONS

Linearizations of unsteady vortex-lattice aerodynamics have been shown to provide a general framework for time-domain representations of the aerodynamic loading in aeroelasticity at low-Mach (incompressible) speeds. The description naturally results in a linear time-invariant discrete-time state-state formulation suitable for feedback connection with structural dynamics in either modal or physical coordinates. Nondimensionalization of the equations scales the description with the dynamic pressure, thus overcoming the need for re-evaluation of the coefficients at different flight conditions (e.g., for flutter analysis). The linearization has been perfor-

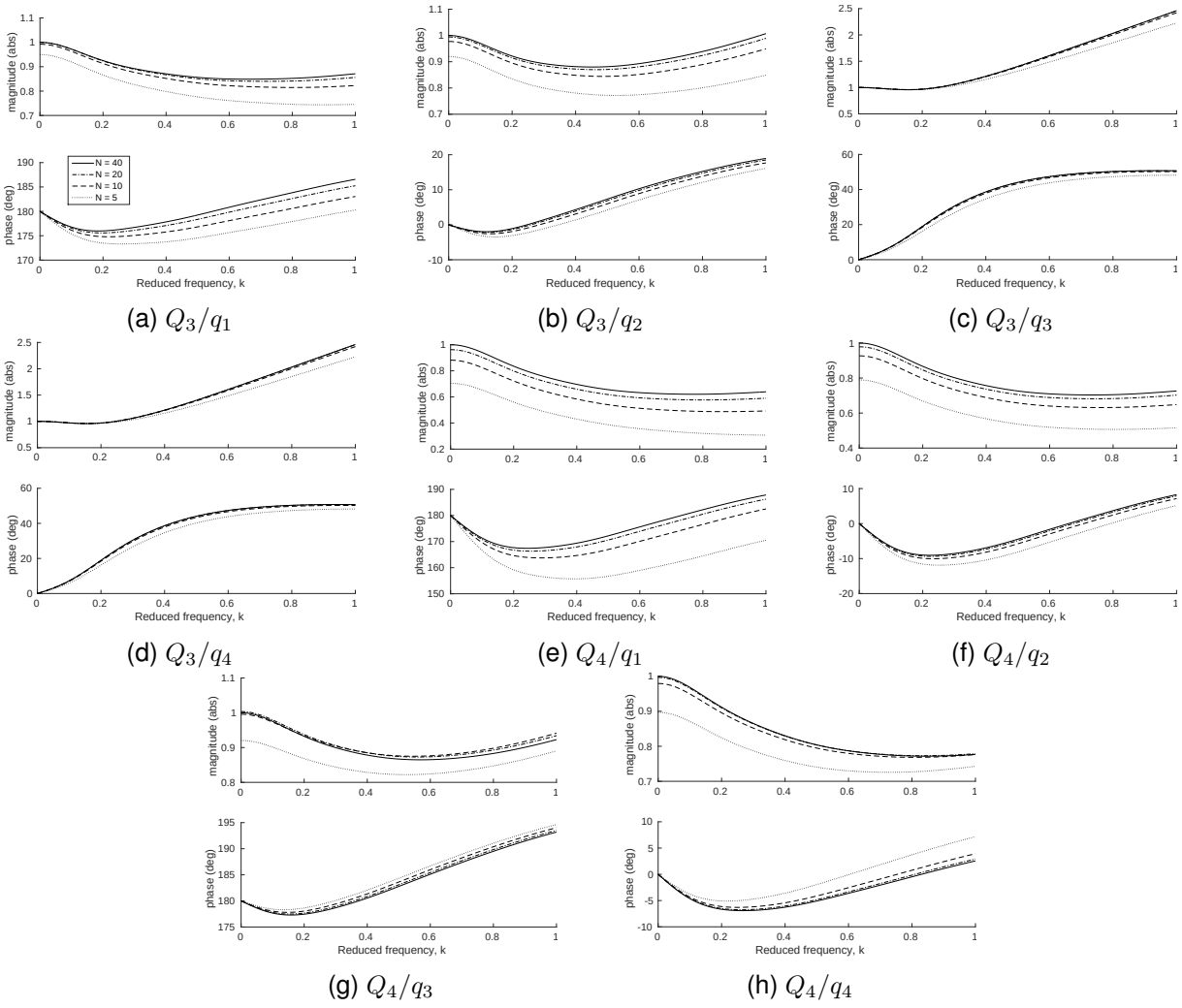

Figure 8: Full-order model frequency responses of the Goland wing aerodynamics for inputs in the first four aeroelastic modes and outputs in the third and fourth modes. Amplitudes normalized by the $N = 40$ steady-state values. Chordwise discretization is $M = 20$, $M_w = 200$.

med around non-zero reference conditions, so as to include the effect of induced drag, steady forces, or large wing deformations in equilibrium in the unsteady forces. The large model size due to the wake discretization is tackled by using standard methods of model reduction for linear systems. Here, balance residualization is seen to reduced the size of the system by more than two orders of magnitude without loss of accuracy at the reduced frequencies of interest.

ACKNOWLEDGEMENTS

This work was made possible through funding provided by the UK Engineering and Physical Sciences Research Council grant EP/N006224/1.

6 REFERENCES

[1] Albano, E. and Rodden, W. (1969). A doublet-lattice method for calculating lift distributions on oscillating surfaces in subsonic flows. *AIAA Journal*, 7(2), 279 – 285.

[2] Blair, M. (1992). A compilation of the mathematics leading to the doublet lattice method. Tech. Rep. WL-TR-92-3028, DTIC.

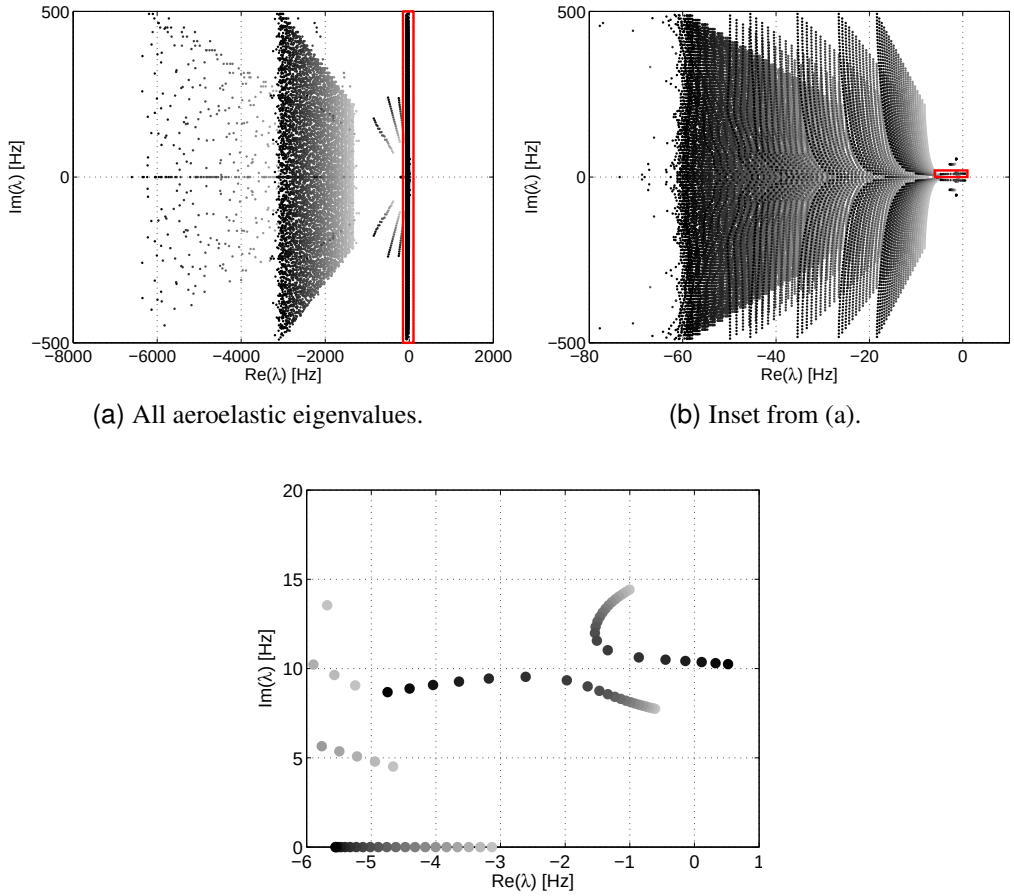

(a) All aeroelastic eigenvalues.

(b) Inset from (a).

(c) Inset from(b).

Figure 9: Continuous-time eigenvalues of the aeroelastic Goland wing model calculated at free-stream velocities $V_\infty = 80, 85, \ldots, 175, 180$ m·s^{-1} (light to dark). Aerodynamic discretization: $M = 10$, $N = 20$, $M_w = 100$. 4 beam modes.

[3] Kier, T. M., Verveld, M. J., and Burkett, C. W. (2015). Flexible Dynamic Loads Models Based on Aerodynamic Influence Coefficients of a 3D Panel Method. Saint Petersburg, Russia.

[4] Hansen, M. O. L., Srensen, J. N., Voutsinas, S., et al. (2006). State of the art in wind turbine aerodynamics and aeroelasticity. *Progress in Aerospace Sciences*, 42(4), 285–330. ISSN 0376-0421. doi:10.1016/j.paerosci.2006.10.002.

[5] Roger, K. L. (1977). Airplane math modelling and active aeroelastic control design. In *AGARD Structures and Materials Panel*. AGARD-CP-228.

[6] Brase, L. O. and Eversman, W. (1988). Application of transient aerodynamics to the structural nonlinear flutter problem. *Journal of Aircraft*, 25(11), 1060 – 1068.

[7] Eversman, W. and Tewari, A. (1991). Consistent rational fraction approximation for unsteady aerodynamics. *Journal of Aircraft*, 28(9), 545–552. doi:10.2514/3.46062.

[8] Hall, K. C. (1994). Eigenanalysis of unsteady flows about airfoils, cascades, and wings. *AIAA Journal*, 32, 2426–2432.

[9] Heeg, J. and Dowell, E. H. (1999). Aerodynamic and aeroelastic iinsights using eigenanalysis. In *40th AIAA/ASME/ASCE/AHS/ASC Structures, Structural Dynamics, and Materials Conference and Exhibit*. St Louis, Missouri, USA.

[10] Heeg, J. and Dowell, E. H. (2001). Characterizing aeroelastic systems using eigenanalysis, explicitly retaining the aerodynamic degrees of freedom. In *42nd AIAA/ASME/ASCE/AHS/ASC Structures, Structural Dynamics and Materials Conference*. Seattle, Washington, USA.

[11] Murua, J., Palacios, R., and Graham, J. M. R. (2012). Applications of the unsteady vortex-lattice method in aircraft aeroelasticity and flight dynamics. *Progress in Aerospace Sciences*, 55, 46–72. doi:10.1016/j.paerosci.2012.06.001.

[12] Murua, J., Martnez, P., Climent, H., et al. (2014). T-tail flutter: Potential-flow modelling, experimental validation and flight tests. *Progress in Aerospace Sciences*, 71, 54–84. doi:10.1016/j.paerosci.2014.07.002.

[13] Baker, M. L., Mingori, D. L., and Goggin, P. J. (1996). Approximate subspace iteration for constructing internally balanced reduced order models of unsteady aerodynamic systems. In *37th AIAA/ASME/ASCE/AHS/ASC Structures, Structural Dynamics and Materials Conference and Exhibit*. Salt Lake City, Utah, USA. AIAA Paper No 1996-1441.

[14] Rule, J. A., Cox, D. E., and Clark, R. L. (2004). Aerodynamic model reduction through balanced realization. *AIAA Journal*, 42(5). doi:10.2514/1.9596.

[15] Hesse, H. and Palacios, R. (2016). Dynamic load alleviation in wake vortex encounters. *Journal of Guidance, Control, and Dynamics*, 39(4), 801–813. doi:10.2514/1.G000715.

[16] Simpson, R. J. S., Palacios, R., and Murua, J. (2013). Induced drag calculations in the unsteady vortex lattice method. *AIAA Journal*, 51(7), 1775 – 1779. doi:10.2514/1.J052136.

[17] Katz, J. and Plotkin, A. (2001). *Low-Speed Aerodynamics*. Cambridge University Press.

[18] Wang, Z., Chen, P. C., Liu, D. D., et al. (2010). Nonlinear-Aerodynamics/Nonlinear-Structure interaction methodology for a high-altitude long-endurance wing. *Journal of Aircraft*, 47(2), 556 – 566.

[19] Murua, J. (2012). *Flexible Aircraft Dynamics with a Geometrically-Nonlinear Description of the Unsteady Aerodynamics*. Ph.D. thesis, Imperial College London, Department of Aeronautics.

[20] Brown, S. A. (1997). Displacement extrapolations for CFD + CSM aeroelastic analysis. In *38th AIAA/ASME/ASCE/AHS/ASC Structures, Structural Dynamics, and Materials Conference*. Kissimmee, Florida.

[21] Meirovitch, L. (1990). *Dynamics and control of structures*. John Wiley & Sons.

[22] Géradin, M. and Cardona, A. (2001). *Flexible Multibody Dynamics: A Finite Element Approach*. Chichester, UK: John Wiley & Sons Ltd.

[23] Sears, W. R. (1941). Some aspects of non-stationary airfoil theory and its practical application. *Journal of the Aeronautical Sciences*, 8(3), 104–108.

[24] Moore, B. (1981). Principal component analysis in linear systems: Controllability, observability, and model reduction. *Automatic Control, IEEE Transactions on*, 26(1), 17–32. doi:10.1109/TAC.1981.1102568.

[25] Goland, M. (1945). The flutter of a uniform cantilever wing. *Journal of Applied Mechanics*, 12(4), A197 – A208.

[26] Hesse, H. and Palacios, R. (2014). Reduced-order aeroelastic models for dynamics of maneuvering flexible aircraft. *AIAA Journal*, 52(8), 1717 – 1732. ISSN 0001-1452. doi: 10.2514/1.J052684.

COPYRIGHT STATEMENT